Thermalization and Sub-Poissonian Density Fluctuations in a Degenerate Molecular Fermi Gas

William G. Tobias, Kyle Matsuda, Giacomo Valtolina, Luigi De Marco, Jun-Ru Li, and Jun Ye

Phys. Rev. Lett. **124**, 033401 — Published 22 January 2020

DOI: 10.1103/PhysRevLett.124.033401

Thermalization and Sub-Poissonian Density Fluctuations in a Degenerate Molecular Fermi Gas

William G. Tobias*, Kyle Matsuda*, Giacomo Valtolina, Luigi De Marco, Jun-Ru Li, and Jun Ye
JILA, National Institute of Standards and Technology and Department of Physics, University of Colorado, Boulder, Colorado 80309, USA
(Dated: December 2, 2019)

We observe thermalization in the production of a degenerate Fermi gas of polar ^{40}K^{87}Rb molecules. By measuring the atom–dimer elastic scattering cross section near the Feshbach resonance, we show that Feshbach molecules rapidly reach thermal equilibrium with both parent atomic species. Equilibrium is essentially maintained through coherent transfer to the ground state. Sub-Poissonian density fluctuations in Feshbach and ground-state molecules are measured, giving an independent characterization of degeneracy and directly probing the molecular Fermi–Dirac distribution.

Degenerate gases of polar molecules, which exhibit long-range, anisotropic dipole-dipole interactions, open new possibilities for engineering strongly-correlated quantum matter [1–9]. Heteronuclear molecules have been produced near quantum degeneracy by magnetoassociation of weakly-bound Feshbach molecules followed by coherent optical transfer to the rovibrational ground state [10–17]. Recently, a degenerate Fermi gas of polar ^{40}K^{87}Rb molecules was realized using this method, starting from a deeply degenerate Bose–Fermi atomic mixture [18]. The degenerate molecules were found to have momentum distributions consistent with thermal equilibrium and exhibited reduced chemical reactivity due to quantum statistics.

Reaching higher phase space density remains an outstanding challenge in ultracold molecule experiments. Multiple factors hinder efficient evaporation of ground-state molecules, including inelastic loss [19, 20] and weak elastic interactions in the absence of an applied electric field [21]. Producing degenerate Feshbach molecules can thus be critically important for creating degenerate ground-state molecules. Feshbach molecule conditions may depend sensitively on atom–dimer thermalization during the molecule association process, which has not been studied in experiment.

Bosonic Feshbach molecules formed in Fermi–Fermi mixtures are observed to reach thermal equilibrium due to strong atom–dimer and dimer–dimer elastic interactions and fermionic suppression of inelastic processes [22–28]. For heteronuclear molecules produced from Bose–Fermi mixtures, the situation is more complex. Inelastic boson–dimer collisions play a larger role [29–31] and atom–dimer elastic scattering has not been previously measured. Characterizing elastic and inelastic processes in these systems is essential for understanding thermalization dynamics and optimizing the production of a low-entropy sample.

In this Letter, we demonstrate that ^{40}K^{87}Rb Feshbach molecules (KRb*) produced from a degenerate Bose–Fermi mixture rapidly come to thermal equilibrium, and that equilibrium is essentially maintained after coherent transfer to ground-state molecules (KRb). To quantify elastic processes during KRb* formation, we measure the magnitude of the atom–dimer scattering length for K–KRb* and Rb–KRb* collisions as a function of the magnetic bias field. We find that the molecular degeneracy saturates as a function of the magnetoassociation ramp rate, indicating that elastic collisions predominate over inelastic collisions and lead to thermalization. As a direct probe of the state occupation of degenerate molecular samples, we additionally measure sub-Poissonian number fluctuations in KRb* and KRb, a technique previously used to characterize degeneracy and phase transitions in atomic gases [32–37]. The momentum distribution in time-of-flight (TOF) expansion and the spatial profile of density fluctuations give consistent results for the molecular T/T_F, where T_F is the Fermi temperature, validating the thermometry of the gas.

We prepare an ultracold mixture of fermionic ^{40}K in the $|F, m_F\rangle = |9/2, -9/2\rangle$ hyperfine state and bosonic ^{87}Rb in the $|1, 1\rangle$ state in a crossed optical dipole trap. The trap frequencies are $(\omega_x, \omega_y, \omega_z) = 2\pi \times (60, 240, 60)$ Hz for K, and are scaled by factors of 0.72, 0.83, and 0.79 for Rb, KRb*, and KRb, respectively. The trap y-axis and the bias magnetic field B are aligned in the direction of gravity. Feshbach molecules are produced by ramping B through the broad interspecies resonance at $B_0 = 546.62$ G (3.04 G width) [38], and can be subsequently transferred to the ground state using stimulated Raman adiabatic passage (STIRAP). Initial atom conditions for optimal molecule production are 5×10^5 K at $T/T_\mathrm{F} = 0.1$ and 6×10^4 Rb at $T/T_\mathrm{c} = 0.5$, resulting in 3×10^4 KRb molecules at $T/T_\mathrm{F} = 0.3$ [18].

The interplay of atom–atom and atom–dimer elastic and inelastic processes, which depend on the detuning from the Feshbach resonance, leads to a complicated evolution of the K–Rb–KRb* mixture during the Feshbach ramp. Inelastic processes in this system have been previously characterized experimentally [29, 30]. Near the Feshbach resonance, free K and Rb atoms are indistinguishable from the weakly-bound molecular constituents, leading to fermionic suppression of inelastic collisions of KRb* with K and bosonic enhancement of those with Rb. In order to minimize inelastic Rb–KRb* losses, the initial

Rb number is chosen so that Rb is no longer condensed after molecule production. After forming molecules, the peak density of K is approximately 10 times larger than Rb, so thermalization of KRb* is expected to occur predominantly through collisions with K. Despite the low Rb density, we expect a small number of Rb-KRb* elastic collisions to occur during the Feshbach ramp; measurements of the Rb-KRb* scattering length are included in the Supplementary Material [39].

Here, we extract the elastic cross section for K–KRb* scattering as a function of B by measuring the damping of KRb* center-of-mass oscillations due to collisions with K. The damping rate is proportional to the elastic collision rate $\Gamma = \overline{n}\sigma v_{\rm rel}$, where $\overline{n} = \left(\frac{1}{N_{\rm K}} + \frac{1}{N_{\rm KRb^*}}\right) \int n_{\rm K} n_{\rm KRb^*}\, d^3x$ is the overlap density between the two species, $n_{\rm K}$ ($n_{\rm KRb^*}$) is the K (KRb*) density distribution, σ is the K–KRb* elastic cross section, and $v_{\rm rel} = \left[\frac{8k_{\rm B}}{\pi}\left(\frac{T_{\rm K}}{m_{\rm K}} + \frac{T_{\rm KRb^*}}{m_{\rm KRb}}\right)\right]^{1/2}$ is the average relative velocity between the two species [40–44]. We assume s-wave atom–dimer collisions, so that $\sigma = 4\pi a_{\rm ad}^2/(1 + k_{\rm th}^2 a_{\rm ad}^2)$, where $a_{\rm ad}$ is the K–KRb* atom–dimer s-wave scattering length, $k_{\rm th} = \sqrt{2\mu k_B T/\hbar^2}$ is the thermal collision wavevector, and μ is the K–KRb* reduced mass [45]. A universal prediction gives $a_{\rm ad} = 1.09a$ near the Feshbach resonance for the mass ratio $m_{\rm K}/m_{\rm Rb} = 0.46$, where a is the K–Rb scattering length [46].

To perform the measurement, we first produce ground-state KRb at $B = 545.5$ G and remove all of the Rb atoms and a fraction of the K atoms using a combination of microwave pulses and light resonant with the atomic transition. A second STIRAP sequence transfers the molecules back to the Feshbach state, producing a sample of 2×10^4 KRb* at $T = 300$ nK and 1.5×10^5 K at $T = 600$ nK. The timing of the two STIRAP pulses is chosen such that the photon recoil selectively excites a center-of-mass oscillation of KRb* [39]. Next, we ramp to the target B in 0.5 ms, and after a variable hold time image the position of KRb* after 6 ms TOF. Due to the large number imbalance between K and KRb*, no induced motion of K is observed. By fitting the decay of the KRb* oscillations, corrected by a small background damping rate due to trap anharmonicity, we obtain a measurement of the collision rate Γ and extract $|a_{\rm ad}|$. The upper panel of Fig. 1 shows the KRb* oscillations at a field of $B = 546.1$ G with varying overlap density $\overline{n}$. Over nearly a factor of four in $\overline{n}$, we extract consistent values of $|a_{\rm ad}|$. Since K is initially much hotter than KRb*, KRb* rapidly heats to the temperature of K. Measuring the timescale of this heating gives a consistent measurement of the atom–dimer cross section [39].

The results are summarized in the lower panel of Fig. 1, which shows the extracted $|a_{\rm ad}|$ as a function of $B - B_0$. We perform measurements in the region $a < 2000a_0$ ($B - B_0 < -0.3$ G), where the average collision energy

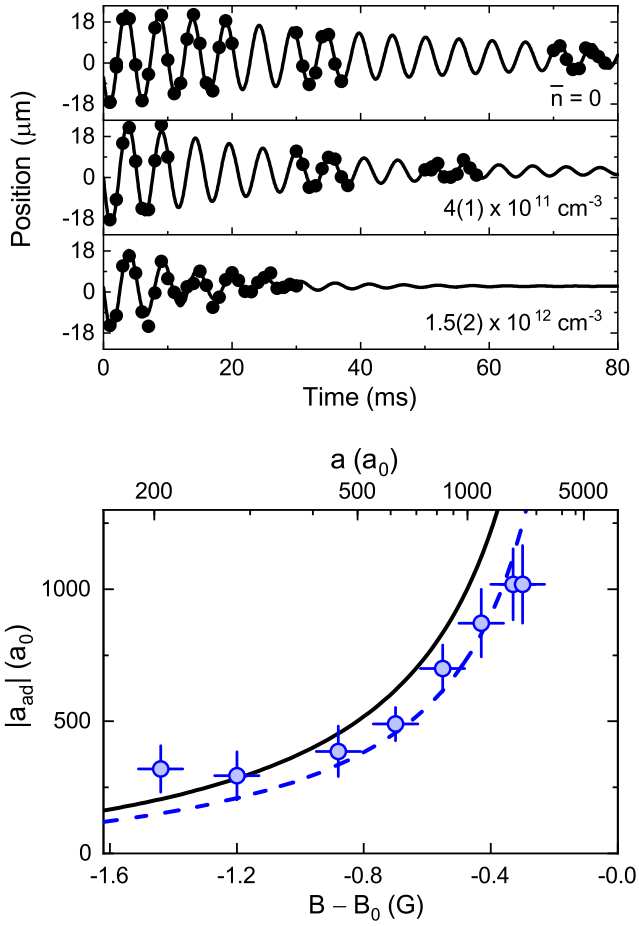

FIG. 1. Upper panel: example oscillations of KRb* at $B = 546.1$ G, varying the overlap density $\overline{n}$. The values of $|a_{\rm ad}| = 684(110)a_0$ and $648(88)a_0$ extracted from the middle and bottom data, respectively, are in good agreement. Lower panel: $|a_{\rm ad}|$ vs $B - B_0$. Dashed line is a fit to the experimental data; see main text. For comparison, the K–Rb scattering length $a(B)$ is shown (solid line). The overlap density for these measurements is $\overline{n} = 1.0(1)\times10^{12}$ cm^{-3}. Vertical error bars denote the standard error; horizontal error bars reflect a small settling of B during the hold time.

is lower than the binding energy. The measured $|a_{\rm ad}|$ as a function of B is fit with a single parameter c, which accounts for a scaling $|a_{\rm ad}| = ca$. The best fit gives $c = 0.74(5)$. Due to the high collision energy and relatively low atom–atom scattering lengths considered here, we do not necessarily expect that the universal prediction $a_{\rm ad} = 1.09a$ holds [46]. Nonetheless, we measure a large atom–dimer scattering length whose magnitude increases near the resonance. An estimate using our typical atomic and molecular densities and the measured $|a_{\rm ad}|$ suggests more than 6 elastic collisions per molecule occur during a 5 ms Feshbach ramp from 555 G to 545.5 G (1.9 G/ms ramp rate), enabling thermalization [39].

Varying the Feshbach ramp rate provides an addi-

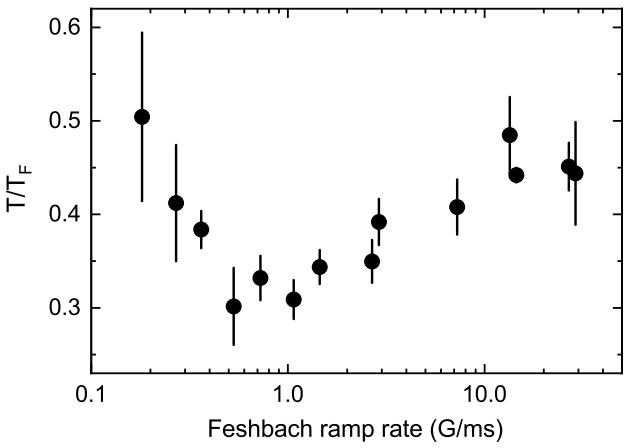

FIG. 2. KRb T/T_F vs Feshbach ramp rate. Error bars denote the standard error. The most degenerate molecules are created with intermediate ramp rates of 0.5–3 G/ms.

tional method for probing the balance between elastic and inelastic scattering rates [22]. In the molecule creation process, there is a competition between thermalization, which favors slower ramp rates, and inelastic losses, which are minimized with faster ramp rates. Figure 2 shows the T/T_F of the KRb cloud, measured by fitting the shape of the cloud after TOF expansion, as a function of the B ramp rate. For intermediate ramp rates of 0.5–3 G/ms, T/T_F reaches a minimum at 0.3. At very slow ramp rates (< 0.5 G/ms), we observe substantial loss from inelastic processes, resulting in a sharp increase in the molecular T/T_F. We also observe a gradual rise in T/T_F as the ramp time becomes much shorter than the trap oscillation period, while the molecule number remains constant, suggesting that thermalization is hindered for fast ramp speeds.

To confirm that the molecules are in thermal equilibrium, we measure the number fluctuations in the gas as an independent probe of T/T_F. Within a subvolume of a classical gas at any temperature, fluctuations are Poissonian, meaning the particle number variance over many experimental repetitions is equal to the mean: $\sigma_N^2/\overline{N} = 1$. In the case of a Fermi gas with $T/T_F \ll 1$, where nearly all states below the Fermi energy are singly occupied, the peak variance is suppressed below the mean by the factor $(3/2)T/T_F$ [34]. The quantity $\sigma_N^2/\overline{N}$ is therefore directly related to the degeneracy of the sample and provides a local measurement of state occupation.

The T/T_F of molecules has so far been measured by fitting the momentum distribution after free expansion. The result is in good agreement with the ratio of the measured temperature and the T_F calculated from the molecule number and trap frequencies. One important consideration for thermometry of ground-state molecules is the effect of STIRAP, which uniformly introduces a small number of holes in the KRb state distribution while preserving the shape of the expanded cloud. Here, we validate expansion thermometry by measuring local number fluctuations in degenerate molecular gases, and show that STIRAP has only a small effect on the molecular state occupation even for the lowest temperatures achieved.

We perform measurements of number fluctuations on K, KRb*, and KRb after 6 ms of free expansion [39]. For measurements on KRb, two successive STIRAP sequences are used: the first converts KRb* to KRb and the second converts KRb to KRb* for imaging prior to TOF expansion. The total duration of the two STIRAP sequences is 270 μs, short enough that inelastic losses between KRb and the remaining atoms are negligible [19]. In order to accurately count the molecule number, we adiabatically dissociate KRb* during expansion with a 2.5 G/ms ramp of B before imaging [47]. Sub-Poissonian number fluctuations have not been previously observed in molecules, making characterization of the imaging system and of the data analysis procedure essential. We use measurements on degenerate and non-degenerate K atoms to benchmark the experimental methods against previous studies on atomic Fermi gases [34, 35].

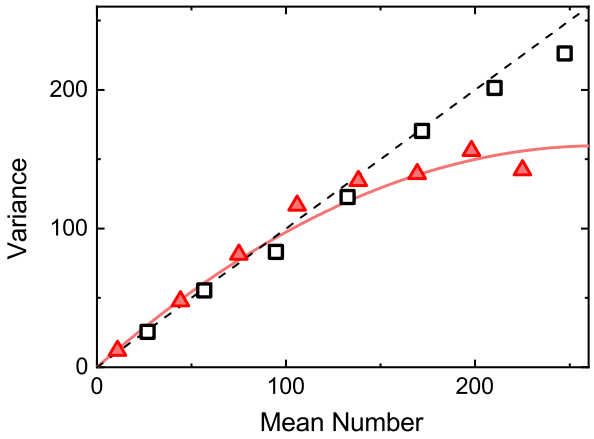

FIG. 3. Variance vs. mean number for non-degenerate K (open squares) and degenerate KRb (solid triangles), averaged over bins with similar mean number. The dashed line indicates equal mean and variance, the expected result for classical particles, and the solid curve is a guide to the eye.

We post-select images to reduce shot-to-shot variation by automatically discarding outliers in total number and temperature, and do not manually exclude any images. Final analysis is performed on 50–60 absorption images of each species. We subdivide the images into bins and fit each to the Fermi–Dirac momentum distribution. Subtracting each fitted profile from the raw optical density profile normalizes against total particle number fluctuations, which would otherwise be the dominant contribution to the variance. By additionally subtracting technical sources of variance—photon shot noise, camera readout noise, and saturation corrections—we obtain the particle number mean and variance for each bin in the set

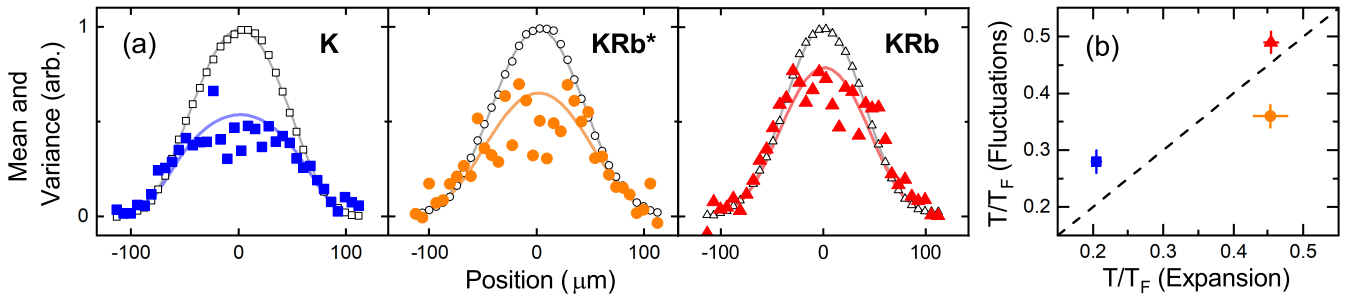

FIG. 4. (a) Mean (open symbols) and variance (solid symbols) profiles, in units of maximum particle number per bin, for K, KRb*, and KRb, averaged over the central 30 camera pixels of each image in the z-direction. Solid lines are fits of the mean and variance to the Fermi-Dirac distribution and Eq. (1), respectively, used to independently determine the T/T_F of each set of images. (b) Comparison between T/T_F extracted from both fitting methods for K (square), KRb* (circle) and KRb (triangle). Dashed line indicates equal T/T_F between the two methods. In both panels, KRb variance is not corrected for STIRAP effects (see main text). Error bars are statistical and correspond to standard errors of the mean.

of images. The measured variance is scaled up to account for imaging resolution and depth-of-field effects, using a scaling factor of 2.2 determined from experimental measurements and simulations of non-degenerate K [39]. Finally, we compute $\sigma_N^2/\overline{N}$ for each bin across all images and compare it to theoretical predictions in order to extract the average T/T_F of the set of images.

Figure 3 shows the dependence of number variance on mean number for degenerate KRb and non-degenerate K. In the non-degenerate case, the variance has linear scaling with mean number over the entire gas, the result expected from Poissonian statistics. By contrast, the degenerate KRb exhibits non-linear scaling of fluctuations, which separate into two distinct regimes. At the edge of the cloud, corresponding to bins with the lowest mean molecule number, the fluctuations are Poissonian due to high availability of unfilled states near the Fermi surface. At the center of the cloud, corresponding to bins with the highest mean molecule number, the fluctuations are sub-Poissonian since most states are filled.

Integrating the particle density in the imaging direction and using the local density approximation, the spatial profile of the variance suppression is given by

$$\frac{\sigma_N^2}{\overline{N}} = \frac{\mathrm{Li}_1(-\zeta e^{-V(x,z)/k_BT})}{\mathrm{Li}_2(-\zeta e^{-V(x,z)/k_BT})}, \qquad (1)$$

where ζ is the peak fugacity, $V(x,z)$ is the optical potential in the imaging plane (scaled by the TOF), and Li_i is the polylogarithm function of order i [35]. Since here $V(x,z)$ is harmonic, *in situ* number fluctuations are preserved in TOF [34]. Figure 4(a) shows profiles of the mean and variance for each species, obtained in separate experimental runs. The suppression is largest at the center of the gas and is reduced approaching the edges, due to the spatial profile of the trapping potential. Independent measures of T/T_F are obtained by (i) fitting the cloud profile in expansion or (ii) fitting the variance suppression to Eq. (1) and extracting ζ. Comparing the T/T_F fit from both methods, we find close agreement for all species across a large range of T/T_F (Fig. 4(b)).

STIRAP transfers KRb* to KRb with a measured efficiency of 85%, producing a slightly out-of-equilibrium initial KRb distribution and increasing the observed number fluctuations. In the general case of molecule formation in bialkali atomic mixtures, STIRAP efficiency poses a technical limitation on degeneracy in the absence of ground-state molecule thermalization [39]. For KRb* with $T/T_F = 0.4$, the occupation fraction of the lowest-energy state in the trap is approximately 0.77. After the application of STIRAP, treated as a binomial process with uniform conversion efficiency over the entire molecular distribution, the occupation fraction is reduced by 15%. The resulting increase in number fluctuations corresponds to a 17% increase in T/T_F [39]. For these conditions, the effect of STIRAP is small since the number of thermal holes is still significant.

When KRb is transferred back to KRb* for imaging, the second STIRAP sequence introduces additional holes; however, since the physical KRb distribution is not affected, this is an imaging artifact and can be corrected [39]. Accounting for the added variance reduces the KRb T/T_F extracted from Eq. (1) from 0.49(2) to 0.44(2). As shown from the comparison to expansion profile fitting in Fig. 4(b), the overall effect of STIRAP on the state occupation is minimal.

We have shown that atom–dimer elastic collision processes thermalize Feshbach molecules during conversion and enable the production of a degenerate molecular Fermi gas at equilibrium. Sub-Poissonian density fluctuations measured in degenerate Feshbach and ground-state molecules provide independent thermometry and a consistent picture of thermal equilibrium. In future experiments on polar molecular gases, local measurement of fluctuations could be used as a sensitive probe of many-body correlations.

We are grateful to E. Cornell, J. D'Incao, P. He, K.-

K. Ni, A.M. Rey, and in particular W. Ketterle and C. Sanner, for stimulating discussions. This work was supported by DARPA DRINQS, ARO-MURI, AFOSR-MURI, NIST, and NSF PHY-1734006.

*W.G.T. and K.M. contributed equally to this work.

[1] A. Micheli, G. K. Brennen, and P. Zoller, Nat. Phys. **2**, 341 (2006).

[2] M. A. Baranov, M. Dalmonte, G. Pupillo, and P. Zoller, Chem. Rev. **112**, 5012 (2012).

[3] K. R. A. Hazzard, S. R. Manmana, M. Foss-Feig, and A. M. Rey, Phys. Rev. Lett. **110**, 075301 (2013).

[4] N. Y. Yao, A. V. Gorshkov, C. R. Laumann, A. M. Läuchli, J. Ye, and M. D. Lukin, Phys. Rev. Lett. **110**, 185302 (2013).

[5] S. V. Syzranov, M. L. Wall, V. Gurarie, and A. M. Rey, Nat. Commun. **5**, 5391 (2014).

[6] M. A. Baranov, M. S. Mar'enko, V. S. Rychkov, and G. V. Shlyapnikov, Phys. Rev. A **66**, 013606 (2002).

[7] T. Miyakawa, T. Sogo, and H. Pu, Phys. Rev. A **77**, 061603(R) (2008).

[8] V. Veljić, A. R. P. Lima, L. Chomaz, S. Baier, M. J. Mark, F. Ferlaino, A. Pelster, and A. Balaž, New Journal of Physics **20**, 093016 (2018).

[9] B. Yan, S. A. Moses, B. Gadway, J. P. Covey, K. R. A. Hazzard, A. M. Rey, D. S. Jin, and J. Ye, Nature **501**, 521525 (2013).

[10] K.-K. Ni, S. Ospelkaus, M. H. G. de Miranda, A. Pe'er, B. Neyenhuis, J. J. Zirbel, S. Kotochigova, P. S. Julienne, D. S. Jin, and J. Ye, Science **322**, 231 (2008).

[11] T. Takekoshi, L. Reichsöllner, A. Schindewolf, J. M. Hutson, C. R. Le Sueur, O. Dulieu, F. Ferlaino, R. Grimm, and H.-C. Nägerl, Phys. Rev. Lett. **113**, 205301 (2014).

[12] P. K. Molony, P. D. Gregory, Z. Ji, B. Lu, M. P. Köppinger, C. R. Le Sueur, C. L. Blackley, J. M. Hutson, and S. L. Cornish, Phys. Rev. Lett. **113**, 255301 (2014).

[13] J. W. Park, S. A. Will, and M. W. Zwierlein, Phys. Rev. Lett. **114**, 205302 (2015).

[14] M. Guo, B. Zhu, B. Lu, X. Ye, F. Wang, R. Vexiau, N. Bouloufa-Maafa, G. Quéméner, O. Dulieu, and D. Wang, Phys. Rev. Lett. **116**, 205303 (2016).

[15] T. M. Rvachov, H. Son, A. T. Sommer, S. Ebadi, J. J. Park, M. W. Zwierlein, W. Ketterle, and A. O. Jamison, Phys. Rev. Lett. **119**, 143001 (2017).

[16] F. Seeßelberg, N. Buchheim, Z.-K. Lu, T. Schneider, X.-Y. Luo, E. Tiemann, I. Bloch, and C. Gohle, Phys. Rev. A **97**, 013405 (2018).

[17] H. Yang, D.-C. Zhang, L. Liu, Y.-X. Liu, J. Nan, B. Zhao, and J.-W. Pan, Science **363**, 261 (2019).

[18] L. De Marco, G. Valtolina, K. Matsuda, W. G. Tobias, J. P. Covey, and J. Ye, Science **363**, 853 (2019).

[19] S. Ospelkaus, K.-K. Ni, D. Wang, M. H. G. de Miranda, B. Neyenhuis, G. Quéméner, P. S. Julienne, J. L. Bohn, D. S. Jin, and J. Ye, Science **327**, 853 (2010).

[20] M. Mayle, G. Quéméner, B. P. Ruzic, and J. L. Bohn, Phys. Rev. A **87**, 012709 (2013).

[21] G. Quéméner and J. L. Bohn, Phys. Rev. A **83**, 012705 (2011).

[22] M. Greiner, C. A. Regal, and D. S. Jin, Nature **426**, 537 (2003).

[23] C. A. Regal, M. Greiner, and D. S. Jin, Phys. Rev. Lett. **92**, 083201 (2004).

[24] S. Jochim, M. Bartenstein, A. Altmeyer, G. Hendl, C. Chin, J. H. Denschlag, and R. Grimm, Phys. Rev. Lett. **91**, 240402 (2003).

[25] M. W. Zwierlein, C. A. Stan, C. H. Schunck, S. M. F. Raupach, A. J. Kerman, and W. Ketterle, Phys. Rev. Lett. **92**, 120403 (2004).

[26] K. E. Strecker, G. B. Partridge, and R. G. Hulet, Phys. Rev. Lett. **91**, 080406 (2003).

[27] M. Jag, M. Zaccanti, M. Cetina, R. S. Lous, F. Schreck, R. Grimm, D. S. Petrov, and J. Levinsen, Phys. Rev. Lett. **112**, 075302 (2014).

[28] M. Jag, M. Cetina, R. S. Lous, R. Grimm, J. Levinsen, and D. S. Petrov, Phys. Rev. A **94**, 062706 (2016).

[29] J. J. Zirbel, K.-K. Ni, S. Ospelkaus, J. P. D'Incao, C. E. Wieman, J. Ye, and D. S. Jin, Phys. Rev. Lett. **100**, 143201 (2008).

[30] R. S. Bloom, M.-G. Hu, T. D. Cumby, and D. S. Jin, Phys. Rev. Lett. **111**, 105301 (2013).

[31] J. Johansen, B. J. DeSalvo, K. Patel, and C. Chin, Nat. Phys. **13**, 731 (2017).

[32] J. Esteve, J.-B. Trebbia, T. Schumm, A. Aspect, C. I. Westbrook, and I. Bouchoule, Phys. Rev. Lett. **96**, 130403 (2006).

[33] N. Gemelke, X. Zhang, C.-L. Hung, and C. Chin, Nature **460**, 995 (2009).

[34] C. Sanner, E. J. Su, A. Keshet, R. Gommers, Y.-i. Shin, W. Huang, and W. Ketterle, Phys. Rev. Lett. **105**, 040402 (2010).

[35] T. Müller, B. Zimmermann, J. Meineke, J.-P. Brantut, T. Esslinger, and H. Moritz, Phys. Rev. Lett. **105**, 040401 (2010).

[36] A. Amico, F. Scazza, G. Valtolina, P. E. S. Tavares, W. Ketterle, M. Inguscio, G. Roati, and M. Zaccanti, Phys. Rev. Lett. **121**, 253602 (2018).

[37] A. Omran, M. Boll, T. A. Hilker, K. Kleinlein, G. Salomon, I. Bloch, and C. Gross, Phys. Rev. Lett. **115**, 263001 (2015).

[38] C. Klempt, T. Henninger, O. Topic, M. Scherer, L. Kattner, E. Tiemann, W. Ertmer, and J. J. Arlt, Phys. Rev. A **78**, 061602(R) (2008).

[39] See Supplementary Materials (including Refs. [48–52]) at xxxxx for additional details.

[40] P. Maddaloni, M. Modugno, C. Fort, F. Minardi, and M. Inguscio, Phys. Rev. Lett. **85**, 2413 (2000).

[41] S. D. Gensemer and D. S. Jin, Phys. Rev. Lett. **87**, 173201 (2001).

[42] G. Ferrari, M. Inguscio, W. Jastrzebski, G. Modugno, G. Roati, and A. Simoni, Phys. Rev. Lett. **89**, 053202 (2002).

[43] F. Ferlaino, R. J. Brecha, P. Hannaford, F. Riboli, G. Roati, G. Modugno, and M. Inguscio, J. Opt. B **5**, S3 (2003).

[44] D. Naik, A. Trenkwalder, C. Kohstall, F. M. Spiegelhalder, M. Zaccanti, G. Hendl, F. Schreck, R. Grimm, T. M. Hanna, and P. S. Julienne, Eur. Phys. J. D **65**, 55 (2011).

[45] C. Chin, R. Grimm, P. Julienne, and E. Tiesinga, Rev. Mod. Phys. **82**, 1225 (2010).

[46] D. S. Petrov, Phys. Rev. A **67**, 010703(R) (2003).

[47] T. Mukaiyama, J. R. Abo-Shaeer, K. Xu, J. K. Chin, and W. Ketterle, Phys. Rev. Lett. **92**, 180402 (2004).

[48] C. R. Monroe, E. A. Cornell, C. A. Sackett, C. J. Myatt,

and C. E. Wieman, Phys. Rev. Lett. **70**, 414 (1993).
[49] H. Wu and C. J. Foot, J. Phys. B **29**, L321 (1996).
[50] A. Mosk, S. Kraft, M. Mudrich, K. Singer, W. Wohlleben, R. Grimm, and M. Weidemüller, Applied Physics B **73**, 791 (2001).
[51] K. Hueck, N. Luick, L. Sobirey, J. Siegl, T. Lompe, H. Moritz, L. W. Clark, and C. Chin, Opt. Express **25**, 8670 (2017).
[52] G. Reinaudi, T. Lahaye, Z. Wang, and D. Guéry-Odelin, Opt. Lett. **32**, 3143 (2007).